

Single-cell full-length spatial transcriptomics reveal the unexplored isoform diversity of the myocardium post-MI

Etienne Boileau^{1,2,3}, Xue Li^{2,3}, Christian Becker⁴, Ramona Casper⁴, Janine Altmüller⁵, Florian Leuschner^{2,3}, Christoph Dieterich^{1,2,3}

¹Section of Bioinformatics and Systems Cardiology, Klaus Tschira Institute for Integrative Computational Cardiology, Im Neuenheimer Feld 669, 69120 Heidelberg, Germany

²Department of Internal Medicine III (Cardiology, Angiology, and Pneumology), University Hospital Heidelberg, Im Neuenheimer Feld 669, 69120 Heidelberg, Germany

³DZHK (German Centre for Cardiovascular Research) Partner Site Heidelberg/Mannheim

⁴Cologne Center for Genomics (CCG), University of Cologne, Weyertal 115b, 50931 Cologne, Germany

⁵Berlin Institute of Health at Charité-Universitätsmedizin Berlin, Max Delbrück Center for Molecular Medicine

Correspondence*:

Christoph Dieterich

christoph.dieterich@uni-heidelberg.de

2 ABSTRACT

3 We introduce Single-cell Nanopore Spatial Transcriptomics (scNAST), a set of tools to facilitate
4 the analysis of spatial gene expression from second- and third-generation sequencing, allowing
5 to generate a full-length single-cell transcriptional landscape of the tissue microenvironment.
6 Taking advantage of the Visium Spatial platform, we adapted a strategy recently developed to
7 assign barcodes to long-read single-cell sequencing data for spatial capture technology. Here, we
8 demonstrate our workflow using four short axis sections of the mouse heart following myocardial
9 infarction. We constructed a *de novo* transcriptome using long-read data, and successfully
10 assigned 19794 transcript isoforms in total, including clinically-relevant, but yet uncharacterized
11 modes of transcription, such as intron retention or antisense overlapping transcription. We showed
12 a higher transcriptome complexity in the healthy regions, and identified intron retention as a
13 mode of transcription associated with the infarct area. Our data revealed a clear regional isoform
14 switching among differentially used transcripts for genes involved in cardiac muscle contraction
15 and tissue morphogenesis. Molecular signatures involved in cardiac remodeling integrated with
16 morphological context may support the development of new therapeutics towards the treatment
17 of heart failure and the reduction of cardiac complications.

18 **Keywords:** Spatial transcriptomics, Single-cell RNA sequencing, Oxford Nanopore Technology, Myocardial Infarction

INTRODUCTION

Cell type heterogeneity has recently emerged as a major aspect in redrawing the cellular picture of the mammalian heart (Wang et al., 2020; Tucker et al., 2020; Litviňuková et al., 2020). Single-cell RNA-seq (scRNA-seq) technology has enabled to explore crosstalk of different cardiac cell populations to identify response signatures involved in remodeling after myocardial infarction (MI) and ischemic injury (Cui et al., 2020; Forte et al., 2020; Ruiz-Villalba et al., 2020; Vafadarnejad et al., 2020; Molenaar et al., 2021; Gladka et al., 2021; Tombor et al., 2021; Heinrichs et al., 2021). These and other data provide a valuable compendium of information to better understand transcriptional changes occurring in cardiomyocyte and non-cardiomyocyte sub-populations in healthy, injured, and regenerating hearts. However, in all these studies, the original tissue architecture is destroyed and, in general, the morphological context is lost, including the relationship of cells to infarct, border and remote zones (van Duijvenboden et al., 2019a).

Recent development in spatial transcriptomics addresses this challenge, but few studies only have provided spatially resolved insights into the cardiac transcriptome. Techniques such as microdissection (Wu et al., 2016; Burkhard and Bakkers, 2018) or, in particular, spatially barcoded arrays and *in situ* capturing, have enabled to retain the spatial information while profiling the whole transcriptome at near single-cell resolution, allowing to shed light on localized tissue neighbourhoods (Asp et al., 2017, 2019), but a detailed characterization of cellular zones of injury, repair and/or remodeling is lacking. MI is a complex spatio-temporal heterogeneous disease involving the whole heart, and unbiased spatial transcriptomics holds a promise to add tissue context to molecular profiling in the search of novel therapeutics.

One of the most established spatial transcriptomics methods is now widely available as the Visium platform by 10x Genomics. After the tissue section is fixed on the spatial slide, stained, and imaged, it is permeabilized to release RNA to bind to capture probes for on-slide cDNA synthesis. Library preparation is performed off-slide, and spatial barcodes and tissue image are used to overlay transcriptomics data with tissue context. Although several new such methods have recently been published (Rodrigues et al., 2019; Liu et al., 2020), they are for the most part relying on short-read library preparation. Thus they are subject to amplification biases and fail to generate sufficient overlaps to reconstruct transcriptomes *de novo*.

Adequate gene and transcript models are instrumental towards relevant proof of concepts and investigational new drug development in translational cardiac research (Müller et al., 2021). Third-generation or long-read sequencing allow to reconstruct truthful assemblies with fewer gaps and to characterize complete transcript isoforms and chimeric transcripts. This has recently been taken to the single-cell level using either Pacific Biosciences (PacBio) or Oxford Nanopore technology (Gupta et al., 2018; Lebrigand et al., 2020; Volden and Vollmers, 2021; Wang et al., 2021; Joglekar et al., 2021).

Here, taking advantage of the conceptual similarity between spatial and cell barcodes, we introduce Single-cell Nanopore Spatial Transcriptomics (SCNAST), a set of tools to facilitate whole transcriptome spatial profiling of full-length transcripts, based on a previously published Bayesian approach for cell barcode assignment (Wang et al., 2021). Our method relies on the commercially available Visium platform by 10x Genomics and Nanopore long-read sequencing, although it can in principle be extended to other technologies, as long as a hybrid sequencing approach is used for spatial barcode assignment.

In this short report, we demonstrate how SCNAST can be used to characterize the spatial transcriptional landscape of the heart post-MI. Using our workflow, we were able to assign a total of 7616 spatial spots across four short axis sections of the heart, corresponding to distinct 19794 transcript isoforms in total, encoded by 12474 genes. We showed a higher transcriptome complexity in the healthy regions, and identified intron retention as a mode of transcription associated with the injured areas. Our results showed a

61 clear regional isoform switching among differentially used transcripts for genes involved in cardiac muscle
62 contraction and tissue morphogenesis, many of them clinically relevant, opening new opportunities in
63 translational cardiac research.

MATERIAL AND METHODS

64 Experimental model of myocardial infarction

65 A C57BL/6 mouse (female, 8 weeks old, Janvier Labs) was exposed to 5% isoflurane for anesthesia. An
66 intubation cannula was inserted orally into the trachea. The mouse was fixed on a heating plate at 37°C
67 and maintained under anesthesia with 2% isoflurane. An incision was made from the left sternum to the
68 midclavicular line. Skins and muscle layers were stretched with forceps and sutures. Another incision was
69 made between the third and fourth intercostal space. The heart was exposed and subjected to permanent
70 myocardial infarction with ligation of the left anterior descending (LAD) coronary artery. When the ribs
71 and skins were fully closed, the isoflurane supply was cut off. Oxygen was then supplied until normal
72 breathing was resumed.

73 Heart extraction and cryosection

74 Three days after permanent LAD ligation, the mouse was sacrificed for organ harvest. After washing with
75 cold PBS several times to remove the blood, the heart was transferred into a bath of isopentane (Millipore
76 Sigma) frozen by liquid nitrogen. The freshly obtained heart was kept fully submerged in isopentane
77 for 5 min until fully frozen. Pre-cooled Cryomold on the dry ice was filled with chilled TissueTek OCT
78 compound without introducing bubbles. The frozen tissue was then transferred into the OCT with pre-
79 cooled forceps and placed on the dry ice until the OCT was completely frozen. OCT-embedded tissue
80 blocks were removed from the Cryomold and mounted on the specimen stage. 10µm sections were cut in
81 a cryostat at -10°C and placed within a Capture Area on the pre-equilibrated Visium Spatial Slides (10x
82 Genomics). The slides were later sealed in individual 50 ml Falcon at -80°C ready for further processing.

83 10X Genomics Visium experiments

84 Four short axis sections of the heart were processed according to the manufacturer's protocol. Libraries
85 were prepared individually, one per heart section. The Visium Spatial Tissue Optimization Slide & Reagent
86 kit (10x Genomics) was used to optimize permeabilization conditions. Tissue permeabilization was
87 performed for 24 min. Spatially barcoded full-length cDNA was generated using the Visium Spatial Gene
88 Expression Slide & Reagent kit (10x Genomics). A fraction of each cDNA library was used for nanopore
89 sequencing. cDNA amplification was then conducted for 20 cycles of PCR (identified by qPCR), and
90 400µl were used in the 10xGenomics Visium library preparation (100µl per section). The libraries were
91 sequenced on a NovaSeq6000 (Illumina), with 29 bases from read 1 and 90 bases from read 2, at a depth
92 of 160M reads per section (640M reads in total). The raw sequencing data was processed with the 10x
93 Genomics Space Ranger v1.1.2 and mapped to the mm10 genome assembly (mm10-2020-A).

94 Oxford Nanopore sequencing libraries

95 Libraries for nanopore sequencing were prepared according to the manufacturer's protocol for direct
96 cDNA Sequencing (SQK-DCS109 Oxford Nanopore Technologies) with the following minor modifications:
97 The protocol was started with 200ng cDNA with the End-prep step. Final library elution was performed in
98 15µl to have material left for TapeStation analysis and Qubit BR measurement. Four GridIon flow cells

99 (FLO-MIN106) were loaded with 12 μ L libraries (74–115ng) by using a Flow Cell Priming kit EXP-FLP002.
100 Base calling was done with Guppy v5.0.12. The High accuracy (HAC) model was selected for base calling
101 (Q-Score cut-off > 9).

102 Spatial barcode assignment

103 To account for source-specific quality differences, each heart section (Illumina libraries) was processed
104 separately using Scanpy v1.7.2 (Wolf et al., 2018), keeping only spatial barcodes with approximately 150
105 < counts < 18000, 250 < genes < 5000, detected in at least 2 spots, and with less than 40% mitochondrial
106 counts. The resulting datasets were concatenated, normalized, and the union of highly variable genes (per
107 section) were kept for final analysis. Batch balanced KNN (BBKNN) (Polański et al., 2020) with ridge
108 regression (Park et al., 2020) was used for integration and batch correction, starting from a coarse clustering
109 obtained from a BBKNN-corrected graph.

110 For the nanopore libraries, samples were demultiplexed and processed with ScNapBar v1.1.0 using a
111 naive Bayes model to assign spatial barcodes (Wang et al., 2021). Briefly, for each heart section, the Space
112 Ranger results (Illumina libraries) were used to parametrize a model of barcode alignment features to
113 discriminate correct versus false barcode assignment in the nanopore data. FASTQ files were mapped
114 using minimap2 v2.21 (Li, 2018). For transcript isoform quantification, a *de novo* transcriptome annotation
115 was generated. Alignment files were processed by StringTie v2.1.5 in long read mode with the reference
116 annotation to guide the assembly process (Kovaka et al., 2019). The annotations were merge into a non-
117 redundant set of transcripts and compared to the reference using GffCompare v0.12.2 (Pertea and Pertea,
118 2020), after removing single-exon transcripts. To generate feature-spatial barcode matrices, alignment
119 files were split into multiple files, one per spatial barcode, based on the barcode assignments, converted
120 to FASTQ, and aligned to the *de novo* transcriptome with minimap2. Abundances were quantified with
121 Salmon v1.5.2 in alignment-based mode using a long read error model (Patro et al., 2017). Each section
122 was processed separately using Scanpy v1.7.2 and integrated with BBKNN, as described above for the
123 Illumina data. Spatial barcodes were filtered for counts (approximately 50 < counts < 4000), transcripts
124 (approximately 50 < transcripts < 2000, detected in at least 2 spots), and ribosomal genes (< 40%).
125 Neighbors enrichment and cluster co-occurrence analyses were performed using Squidpy (Palla et al., 2021).

126 Identification of anatomical regions

127 For the Illumina libraries, the neighborhood graph was computed using BBKNN. Spots were clustered
128 with a low resolution (0.3) to identify anatomical regions such as infarct, border and remote zones. Marker
129 genes were identified using a Wilcoxon rank sum test with Benjamini–Hochberg correction, by comparing
130 the expression of each gene in a given cluster against the rest of the spots. The final clusters were manually
131 annotated.

132 Labels were then assigned to nanopore spatial barcodes based on the set of matching Illumina barcodes.
133 However, not all assigned barcodes were labeled due to quality control filtering criteria that were different
134 between Illumina and nanopore datasets. To assign labels to the remaining nanopore barcodes, seed
135 labelling was performed with scANVI using the set of assigned labels as groundtruth (Xu et al., 2021). The
136 top expressed transcripts were then identified as described above for the Illumina data.

137 Spatial spot deconvolution

138 Spatial spots were deconvoluted using stereoscope (scvi-tools v0.15.0) (Andersson et al., 2020). Heart
139 data (Smart-Seq2 and 10x Genomics) from the Tabula Muris (Schaum et al., 2018) were used as reference

140 dataset and highly variable genes were identified. For the Smart-Seq2 data, gene length normalization was
141 applied. The model was trained on the single cell reference dataset on the intersection of genes found in
142 the spatial (Illumina) data, and proportions were inferred for each Visium spot for each cell type in the
143 reference dataset. Labels were then assigned to nanopore spots are described above.

144 Spatial gene expression (Illumina)

145 For each heart section, genes with spatial expression patterns were obtained with SPARK (FDR <
146 0.05) (Sun et al., 2020). Overrepresented biological processes in each region were identified using spatially
147 variable markers that were previously identified ($\log FC < 0.2$, p-value < 0.05), using Enrichr with the
148 Python package GSEApY.

149 Differential transcript usage (nanopore)

150 To identify changes in relative usage of transcripts/isoforms within genes, differential transcript usage
151 (DTU) tests were performed using satuRn (Gillis et al., 2021). Only multi-exon transcripts and genes with
152 more than one isoform were kept for the analyses. The transcript count matrix was further filtered to keep
153 transcripts expressed in a worthwhile number of spots, determined by the design (but greater than at least
154 10% of the smallest group size), with a CPM count above a threshold of $1(\text{median library size})^{-1}$. In addition,
155 transcripts were kept only if they had a minimum count of 1 across all spots. A quasi-binomial generalized
156 linear model was fit using a design comparing each anatomical region with another, or each anatomical
157 region with the rest of all regions. A two-stage testing procedure was performed using stageR (Van den
158 Berge and Clement, 2021), with an OFDR of 0.05. Results were reported using a student's t-test statistic,
159 computed with estimated log-odds ratios. To identify isoform-switching genes, significant genes were
160 identified for each contrast with at least two transcripts showing a switching expression pattern between
161 regions of interest.

162 Transcript classes

163 Transcript classes were assigned in scNAST using Gffcompare (Pertea and Pertea, 2020). For the
164 identification of isoforms and transcript classes between regions, markers previously identified were used to
165 select transcripts in each region with a $\log FC > 0.1$ (p-value < 0.05). Enrichment of transcripts of a certain
166 class (e.g. intron retention) was calculated using a Fisher exact test, using only non-equality classes. Motif
167 enrichment was performed using Simple Enrichment Analysis (SEA) from the MEME suite, using retained
168 intron sequences vs. annotated (reference transcript) sequences (Bailey et al., 2015).

RESULTS

169 scNAST enables the demarcation of spatially distinct regions of the myocardium post-MI

170 Fresh-frozen tissue samples were stained, imaged and fixed on Visium Spatial Gene Expression Slides
171 (10X Genomics) for permeabilization and *in situ* RNA capture. Full-length cDNA libraries were split for
172 the preparation of 3' Illumina short-read and direct long-read nanopore sequencing libraries. Short-read
173 data were used for the assignment of spatial barcodes to nanopore reads using the SCNAPBAR workflow,
174 and subsequently used to define anatomical regions within the tissue organization (Fig. 1A). Long-read
175 data were used for transcriptome assembly and transcript abundance quantification, and layered onto the
176 stained images to reveal the spatial organization of isoform expression. The nanopore data comprises of
177 four heart slices (or samples) with a total of 25,5 million reads, reaching a relatively high sequencing

saturation (Fig. 1B), and providing a significant gain in coverage along full-length transcripts (Fig. 1C). After spatial barcode assignment, libraries had a median of 2.8 million reads per sample, with over 70% assigned reads (Figs. 1D and Supplementary Figure S1A). Despite variations across samples, we observed a good per spot correlation between Illumina and nanopore libraries (Fig. Supplementary Figure S1B,C). Per spatial spot ($55\mu\text{m}$), after quality filtering, we observed a median read count varying between 593 and 2021 corresponding to a median of 311 (respectively 1000) distinct isoforms (Fig. Supplementary Figure S2, see also Figs. Supplementary Figure S3 Supplementary Figure S4).

Clustering based on short-read gene expression defined four broad morphological regions: two remote zones that stemmed from differences in sequencing depth between heart slices, a border zone, and the infarct. Remote zones and, to a lesser extent the border zone, were largely associated with cardiomyocyte markers, while the border and infarct zones were characterized by a higher expression of endothelial, myofibroblast, and immune marker genes, as well as with markers of fibrosis and inflammation (Fig. 2A). The region classification was then transferred to the nanopore data (Fig. 2B), and markers of each region were identified (Fig. Supplementary Figure S5). We also investigated, using the Illumina libraries, whether our spatial transcriptomics data reflected known biological processes of myocardial infarction. We identified spatially variable genes across samples and characterized each region using biological processes (Fig. Supplementary Figure S6, and supporting information [Supplementary Table S1](#)). Remote zones were generally associated with cardiac muscle contraction linked to an overrepresentation of healthy cardiomyocytes, and included genes such as *Strit1* (SERCA regulator DWORF), cardiac troponin I (*Tnni3*), myosin-binding protein C (*Mybpc3*), or ventricular myosin light chain-2 (*Myl2*). The border zone was characterized by genes such as *Nppb* or *Ankrd1*, both of which were reported to be upregulated in the border zone after MI (Hama et al., 1995; Mikhailov and Torrado, 2008), and other genes associated with the complement system and myogenesis. Overrepresented processes were however similar to those found in the infarct area. Top markers of the infarct area included collagens and genes associated with TGF- β and p53 signalling, with hypoxia, coagulation, epithelial to mesenchymal transition, and the extracellular matrix. Overrepresented processes included neutrophil degranulation, and gene expression associated with the innate immune system. Remote, border, and infarct zones had a clear distinct spatial organization: the two remote zones co-occurred at short distances with one another, but did not show any neighborhood enrichment with the border and infarct zones (Fig. 2C,D). We observed a slight co-enrichment of the infarct and the border zone at medium distances (Fig. 2D), revealing how spatial resolution may, in general, affect morphological classification.

Following this strategy, we successfully assigned 7616 spatial spots, corresponding to distinct 19794 transcript isoforms in total, encoded by 12474 genes. Among all genes, we observed 8131 (67,3%) that expressed a single isoform and 3953 (32.7%) that expressed 2 or more isoforms (Fig. 2E). Although predicted by our assembly, genes with many isoforms were expressed at a lower threshold and were not included in our final analyses. We observed variations in the number of isoforms per gene across morphological regions of each heart slice, with significant differences between either of the remote zones and the border and the infarct areas, suggesting the existence of a higher transcriptome diversity in the healthy regions (Fig. 2F).

scNAST reveals the spatial isoform diversity of the myocardium post-MI

Transcript isoforms were largely associated with exact matches to the reference annotation, multi-exon transcripts with at least one junction match to the reference (e.g. exon skipping and exon extension), transcripts longer than the reference (containment of reference), completely novel transcripts (intergenic),

transcripts with exonic overlap, intronic transcripts, or retained introns (Fig. 3A). Among these classes, we were particularly interested in novel transcripts associated with retained introns. Intron retention (IR) occurs when an intron is transcribed into pre-mRNA and remains in the final mRNA. Only recently has IR become of interest due to its associations with complex diseases (Zhang et al., 2020). Interestingly, among differentially expressed transcript markers, we found across the infarct and border zones 65 distinct IR transcripts, compared to 1612 in the remote zones, corresponding to an odds ratio of 1.73 (p-value 0.008). When considering the infarct area only, the odds were even greater (odds ratio 2, p-value 0.002). Introns that were retained across the infarct and border zone were enriched in motifs associated with poly(C)-binding protein 1 and 3 (Pcbp1/3), KH RNA-binding domains (Khdrbs1), and Rbm38, a homolog of Rbm24, a pivotal cardiac splice factor (Weeland et al., 2015) (supporting information [Supplementary Table S2](#)). The genes harboring these transcripts were enriched in RNA metabolic/catabolic processes, RNA binding, and the unfolded protein response (Fig. 3B). Among these, we found cardiac muscle alpha actin (Actc1), the major protein of the thin filament responsible for cardiac contraction (Fig. 3C). Our data revealed a relatively high expression of the IR transcript isoform across all regions, but a comparatively greater contribution to the infarct area (Fig. 3D). Interestingly, Actc1 is located between two (antisense) long non-coding RNAs, one of which has recently been described for its role in cardiomyocyte proliferation and cardiac repair (Ponnusamy et al., 2019). At the Actc1 locus, we identified two novel antisense transcripts with a good coverage across all regions (Fig. 3C). There is now growing evidence that antisense-mediated gene regulation is involved in different pathophysiological contexts, including heart disease (Luther, 2005; Zinad et al., 2017; Celik et al., 2019). Using the Tabula Muris (Schaum et al., 2018) as a reference dataset to perform deconvolution, we identified cardiomyocytes, and to a lesser extent, endothelial and myofibroblasts as the predominant origin of these novel antisense isoforms, with a correlation pattern that matched that of the largest Actc1 annotated isoform (Fig. 3E).

scNAST allows to study regional isoform switching with spatial context

Among the multi-isoform genes, we looked for those showing a splicing pattern variation across regions. We identified 109 significant regional isoform switching genes across all comparisons between the remote, border, and infarct areas (OFDR 0.05 at both gene and transcript level, supporting information [Supplementary Table S3](#)). Our results showed a clear regional isoform switching among differentially used transcripts for genes involved in cardiac muscle contraction and tissue morphogenesis, many of them clinically relevant, such as Ankrd1 (Mikhailov and Torrado, 2008), Sparc (McCurdy et al., 2011), or Clu (Turkieh et al., 2019) (Fig. 4A). The largest number of isoform-switching genes were found between the infarct and the remote zones (Fig. 4B). Among them, we found PDZ and LIM domain protein 5 (Pdlim5), a gene encoding for a protein that localizes to the Z-disk by binding to α -actinin, and which has been implicated in dilated cardiomyopathy (Verdonschot et al., 2020) and in heart failure with preserved ejection fraction (Soetkamp et al., 2021). Pdlim5 undergoes extensive splicing in both human and mouse. Our data showed a significant change in isoform usage between two annotated protein-coding isoforms between the infarct and the border or the remote zones (Fig. 4C,D,E). The shorter isoform was mostly found in the border and remote zones, while the longer isoform was significantly, albeit at lower levels, expressed in the infarct area (Fig. 4C,E).

DISCUSSION

scNAST expands the spatial transcriptomics toolbox to third-generation long-read sequencing. scNAST is based on commercially available platforms, and can be used to investigate the isoform landscape of complex

tissue. We presented here a transcriptome-wide approach to explore annotated and *de novo* isoform diversity with morphological context in the mouse heart after myocardial infarction (MI). Our approach opens-up new opportunities to understand the spatial and molecular organization of the heart following injury. The infarcted heart has usually been divided into three zones: the infarct, an ischemic border zone, roughly defined as the area immediately adjacent to the infarct, and a remote zone. Although previous studies showed transcriptional differences between proximal and distal areas to the infarct (van Duijvenboden et al., 2019b), observations were limited to conventional short-read sequencing approaches or were limited in spatial resolution. Our results not only reflected known biological processes of myocardial infarction, but also revealed the spatial organization of gene expression and transcriptome diversity consistent with the underlying biological condition. We identified novel isoforms in clinically relevant loci and regional isoform switches that could play a role in the myocardium post-MI. We envision that our work will serve as a reference for future developments and studies integrating long-read sequencing with spatial gene expression data.

DATA AVAILABILITY

The datasets generated for this study can be found in the [to be deposited at SRA]. Additional information, supporting data and scripts to generate the figures are available at <https://github.com/dieterich-lab/ScNaST>.

CODE AVAILABILITY

SCNAPBAR is publicly available at <https://github.com/dieterich-lab/single-cell-nanopore>.
scNaST is publicly available at <https://github.com/dieterich-lab/ScNaST>.

AUTHOR CONTRIBUTIONS

CD, FL supervised the research and acquired funding. JA planned and supervised Visium experiments and library preparation. XL performed MI experiments and tissue extraction. CB, RC performed Visium experiments and library preparation. EB was in charge of software development, analyzed the data and wrote the manuscript.

FUNDING

EB and CD acknowledge support by the Klaus Tschira Stiftung gGmbH [00.219.2013]. CD acknowledge the DZHK (German Centre for Cardiovascular Research) Partner Site Heidelberg/Mannheim.

CONFLICT OF INTEREST

The authors declare that they have no conflict of interest.

SUPPLEMENTAL DATA

Supplementary Figure S1

scNaST methodology.

- 289 **Supplementary Figure S2**
- 290 Quality control (nanopore).
- 291 **Supplementary Figure S3**
- 292 Quality control (Illumina).
- 293 **Supplementary Figure S4**
- 294 Spatial distribution of UMIs or counts and genes or transcripts.
- 295 **Supplementary Figure S5**
- 296 Top markers of each region.
- 297 **Supplementary Figure S6**
- 298 Enriched processes among spatially variable marker genes.
- 299 **Supplementary Table S1**
- 300 Spatially variable genes.
- 301 **Supplementary Table S2**
- 302 Motif enriched in IR transcripts.
- 303 **Supplementary Table S3**
- 304 Differential transcript usage (isoform-switching genes).

REFERENCES

- 305 Andersson, A., Bergenstråhlé, J., Asp, M., Bergenstråhlé, L., Jurek, A., Fernández Navarro, J., et al.
306 (2020). Single-cell and spatial transcriptomics enables probabilistic inference of cell type topography.
307 *Communications Biology* 3, 565. doi:10.1038/s42003-020-01247-y. PMID: 33037292
- 308 Asp, M., Giacomello, S., Larsson, L., Wu, C., Fürth, D., Qian, X., et al. (2019). A spatiotemporal
309 organ-wide gene expression and cell atlas of the developing human heart. *Cell* 179, 1647–1660.e19.
310 doi:<https://doi.org/10.1016/j.cell.2019.11.025>. PMID: 31835037
- 311 Asp, M., Salmén, F., Ståhl, P. L., Vickovic, S., Felldin, U., Löfling, M., et al. (2017). Spatial detection
312 of fetal marker genes expressed at low level in adult human heart tissue. *Scientific Reports* 7, 12941.
313 doi:10.1038/s41598-017-13462-5. PMID: 29021611
- 314 Bailey, T. L., Johnson, J., Grant, C. E., and Noble, W. S. (2015). The meme suite. *Nucleic acids research*
315 43, W39–W49. doi:10.1093/nar/gkv416. 25953851[pmid]
- 316 Burkhard, S. B. and Bakkers, J. (2018). Spatially resolved rna-sequencing of the embryonic heart
317 identifies a role for wnt/b-catenin signaling in autonomic control of heart rate. *eLife* 7, e31515.
318 doi:10.7554/eLife.31515. PMID: 29400650
- 319 Celik, S., Sadegh, M. K., Morley, M., Roselli, C., Ellinor, P. T., Cappola, T., et al. (2019). Antisense
320 regulation of atrial natriuretic peptide expression. *JCI Insight* 4. doi:10.1172/jci.insight.130978. PMID:
321 31503546
- 322 Cui, M., Wang, Z., Chen, K., Shah, A. M., Tan, W., Duan, L., et al. (2020). Dynamic transcriptional
323 responses to injury of regenerative and non-regenerative cardiomyocytes revealed by single-nucleus

- 324 rna sequencing. *Developmental Cell* 53, 102–116.e8. doi:<https://doi.org/10.1016/j.devcel.2020.02.019>.
325 PMID: 32220304
- 326 Forte, E., Skelly, D. A., Chen, M., Daigle, S., Morelli, K. A., Hon, O., et al. (2020). Dynamic interstitial
327 cell response during myocardial infarction predicts resilience to rupture in genetically diverse mice. *Cell
328 Reports* 30, 3149–3163.e6. doi:<https://doi.org/10.1016/j.celrep.2020.02.008>
- 329 Gilis, J., Vitting-Seerup, K., Van den Berge, K., and Clement, L. (2021). saturn: scalable analysis of
330 differential transcript usage for bulk and single-cell rna-sequencing applications [version 1; peer review:
331 2 approved with reservations]. *F1000Research* 10. doi:10.12688/f1000research.51749.1
- 332 Gladka, M. M., Kohela, A., Molenaar, B., Versteeg, D., Kooijman, L., Monshouwer-Kloots, J., et al. (2021).
333 Cardiomyocytes stimulate angiogenesis after ischemic injury in a zeb2-dependent manner. *Nature
334 Communications* 12, 84. doi:10.1038/s41467-020-20361-3. PMID: 33398012
- 335 Gupta, I., Collier, P. G., Haase, B., Mahfouz, A., Joglekar, A., Floyd, T., et al. (2018). Single-cell
336 isoform rna sequencing characterizes isoforms in thousands of cerebellar cells. *Nature Biotechnology*
337 36, 1197–1202. doi:10.1038/nbt.4259. PMID: 30320766
- 338 Hama, N., Itoh, H., Shirakami, G., Nakagawa, O., ichi Suga, S., Ogawa, Y., et al. (1995). Rapid ventricular
339 induction of brain natriuretic peptide gene expression in experimental acute myocardial infarction.
340 *Circulation* 92, 1558–1564. doi:10.1161/01.CIR.92.6.1558. PMID: 7664440
- 341 Heinrichs, M., Ashour, D., Siegel, J., Büchner, L., Wedekind, G., Heinze, K. G., et al. (2021). The healing
342 myocardium mobilizes a distinct B-cell subset through a CXCL13-CXCR5-dependent mechanism.
343 *Cardiovascular Research* 117, 2664–2676. doi:10.1093/cvr/cvab181. PMID: 34048536
- 344 Joglekar, A., Prjibelski, A., Mahfouz, A., Collier, P., Lin, S., Schlusche, A. K., et al. (2021). A
345 spatially resolved brain region- and cell type-specific isoform atlas of the postnatal mouse brain. *Nature
346 Communications* 12, 463. doi:10.1038/s41467-020-20343-5. PMID: 33469025
- 347 Kovaka, S., Zimin, A. V., Pertea, G. M., Razaghi, R., Salzberg, S. L., and Pertea, M. (2019). Transcriptome
348 assembly from long-read rna-seq alignments with stringtie2. *Genome Biology* 20, 278. doi:10.1186/
349 s13059-019-1910-1. PMID: 31842956
- 350 Lebrigand, K., Magnone, V., Barbry, P., and Waldmann, R. (2020). High throughput error corrected
351 nanopore single cell transcriptome sequencing. *Nature Communications* 11, 4025. doi:10.1038/
352 s41467-020-17800-6. PMID: 32788667
- 353 Li, H. (2018). Minimap2: pairwise alignment for nucleotide sequences. *Bioinformatics* 34, 3094–3100.
354 doi:10.1093/bioinformatics/bty191. PMID: 29750242
- 355 Litviňuková, M., Talavera-López, C., Maatz, H., Reichart, D., Worth, C. L., Lindberg, E. L., et al.
356 (2020). Cells of the adult human heart. *Nature* 588, 466–472. doi:10.1038/s41586-020-2797-4. PMID:
357 32971526
- 358 Liu, Y., Yang, M., Deng, Y., Su, G., Enninful, A., Guo, C. C., et al. (2020). High-spatial-resolution
359 multi-omics sequencing via deterministic barcoding in tissue. *Cell* 183, 1665–1681.e18. doi:<https://doi.org/10.1016/j.cell.2020.10.026>. PMID: 33188776
- 360 Luther, H. P. (2005). Role of endogenous antisense rna in cardiac gene regulation. *Journal of Molecular
361 Medicine* 83, 26–32. doi:10.1007/s00109-004-0613-5. PMID: 15592803
- 363 McCurdy, S. M., Dai, Q., Zhang, J., Zamilpa, R., Ramirez, T. A., Dayah, T., et al. (2011). Sparc mediates
364 early extracellular matrix remodeling following myocardial infarction. *American journal of physiology.
365 Heart and circulatory physiology* 301, H497–H505. doi:10.1152/ajpheart.01070.2010. 21602472[pmid]
- 366 Mikhailov, A. and Torrado, M. (2008). The enigmatic role of the ankyrin repeat domain 1 gene in heart
367 development and disease. *Int J Dev Biol* 52, 811–821. doi:10.1387/ijdb.082655am. PMID: 18956313

- 368 Molenaar, B., Timmer, L. T., Droog, M., Perini, I., Versteeg, D., Kooijman, L., et al. (2021). Single-cell
369 transcriptomics following ischemic injury identifies a role for b2m in cardiac repair. *Communications
370 Biology* 4, 146. doi:10.1038/s42003-020-01636-3. PMID: 33514846
- 371 Müller, T., Boileau, E., Talyan, S., Kehr, D., Varadi, K., Busch, M., et al. (2021). Updated and enhanced
372 pig cardiac transcriptome based on long-read rna sequencing and proteomics. *Journal of Molecular and
373 Cellular Cardiology* 150, 23–31. doi:<https://doi.org/10.1016/j.yjmcc.2020.10.005>. PMID: 33049256
- 374 Palla, G., Spitzer, H., Klein, M., Fischer, D., Schaar, A. C., Kuemmerle, L. B., et al. (2021). Squidpy: a
375 scalable framework for spatial single cell analysis. *bioRxiv* doi:10.1101/2021.02.19.431994
- 376 Park, J.-E., Botting, R. A., Conde, C. D., Popescu, D.-M., Lavaert, M., Kunz, D. J., et al. (2020). A
377 cell atlas of human thymic development defines t cell repertoire formation. *Science* 367, eaay3224.
378 doi:10.1126/science.aay3224
- 379 Patro, R., Duggal, G., Love, M. I., Irizarry, R. A., and Kingsford, C. (2017). Salmon provides fast and bias-
380 aware quantification of transcript expression. *Nature Methods* 14, 417–419. doi:10.1038/nmeth.4197.
381 PMID: 28263959
- 382 Pertea, G. and Pertea, M. (2020). Gff utilities: Gffread and gffcompare [version 1; peer review: 3 approved].
383 *F1000Research* 2020 9, 304. doi:10.12688/f1000research.23297.1. PMID: 32489650
- 384 Polański, K., Young, M. D., Miao, Z., Meyer, K. B., Teichmann, S. A., and Park, J.-E. (2020). Bbknn: Fast
385 batch alignment of single cell transcriptomes. *Bioinformatics* 36, 964–965. doi:10.1093/bioinformatics/
386 btz625. PMID: 31400197
- 387 Ponnusamy, M., Liu, F., Zhang, Y.-H., Li, R.-B., Zhai, M., Liu, F., et al. (2019). Long noncoding rna
388 cpr (cardiomyocyte proliferation regulator) regulates cardiomyocyte proliferation and cardiac repair.
389 *Circulation* 139, 2668–2684. doi:10.1161/CIRCULATIONAHA.118.035832
- 390 Rodrigues, S. G., Stickels, R. R., Goeva, A., Martin, C. A., Murray, E., Vanderburg, C. R., et al. (2019).
391 Slide-seq: A scalable technology for measuring genome-wide expression at high spatial resolution.
392 *Science* 363, 1463–1467. doi:10.1126/science.aaw1219. PMID: 30923225
- 393 Ruiz-Villalba, A., Romero, J. P., Hernández, S. C., Vilas-Zornoza, A., Fortelny, N., Castro-Labrador,
394 L., et al. (2020). Single-cell rna sequencing analysis reveals a crucial role for cthrc1 (collagen triple
395 helix repeat containing 1) cardiac fibroblasts after myocardial infarction. *Circulation* 142, 1831–1847.
396 doi:10.1161/CIRCULATIONAHA.119.044557. PMID: 32972203
- 397 Schaum, N., Karkalias, J., Neff, N. F., May, A. P., Quake, S. R., Wyss-Coray, T., et al. (2018). Single-
398 cell transcriptomics of 20 mouse organs creates a tabula muris. *Nature* 562, 367–372. doi:10.1038/
399 s41586-018-0590-4. PMID: 30283141
- 400 Soetkamp, D., Gallet, R., Parker, S. J., Holewinski, R., Venkatraman, V., Peck, K., et al. (2021).
401 Myofilament phosphorylation in stem cell treated diastolic heart failure. *Circulation Research* 129,
402 1125–1140. doi:10.1161/CIRCRESAHA.119.316311. PMID: 34641704
- 403 Sun, S., Zhu, J., and Zhou, X. (2020). Statistical analysis of spatial expression patterns for spatially
404 resolved transcriptomic studies. *Nature Methods* 17, 193–200. doi:10.1038/s41592-019-0701-7
- 405 Tombor, L. S., John, D., Glaser, S. F., Luxán, G., Forte, E., Furtado, M., et al. (2021). Single cell sequencing
406 reveals endothelial plasticity with transient mesenchymal activation after myocardial infarction. *Nature
407 Communications* 12, 681. doi:10.1038/s41467-021-20905-1. PMID: 33514719
- 408 Tucker, N. R., Chaffin, M., Fleming, S. J., Hall, A. W., Parsons, V. A., Bedi, K. C., et al. (2020).
409 Transcriptional and cellular diversity of the human heart. *Circulation* 142, 466–482. doi:10.1161/
410 CIRCULATIONAHA.119.045401. PMID: 32403949

- 411 Turkieh, A., Porouchani, S., Beseme, O., Chwastyniak, M., Amouyel, P., Lamblin, N., et al. (2019).
412 Increased clusterin levels after myocardial infarction is due to a defect in protein degradation systems
413 activity. *Cell Death & Disease* 10, 608. doi:10.1038/s41419-019-1857-x. PMID: 31406108
- 414 Vafadarnejad, E., Rizzo, G., Krampert, L., Arampatzi, P., Arias-Loza, A.-P., Nazzal, Y., et al. (2020).
415 Dynamics of cardiac neutrophil diversity in murine myocardial infarction. *Circulation Research* 127,
416 e232–e249. doi:10.1161/CIRCRESAHA.120.317200. PMID: 32811295
- 417 Van den Berge, K. and Clement, L. (2021). *stageR: stage-wise analysis of high throughput gene expression*
418 *data in R*. R package version 1.16.0
- 419 van Duijvenboden, K., de Bakker, D. E., Man, J. C., Janssen, R., Günthel, M., Hill, M. C., et al.
420 (2019a). Conserved Nppb border zone switches from mef2- to ap-1-driven gene program.
421 *Circulation* 140, 864–879. doi:10.1161/CIRCULATIONAHA.118.038944. PMID: 31259610
- 422 van Duijvenboden, K., de Bakker, D. E., Man, J. C., Janssen, R., Günthel, M., Hill, M. C., et al.
423 (2019b). Conserved Nppb border zone switches from mef2- to ap-1-driven gene program.
424 *Circulation* 140, 864–879. doi:10.1161/CIRCULATIONAHA.118.038944. PMID: 31259610
- 425 Verdonschot, J. A. J., Robinson, E. L., James, K. N., Mohamed, M. W., Claes, G. R. F., Casas, K.,
426 et al. (2020). Mutations in *pdlim5* are rare in dilated cardiomyopathy but are emerging as potential
427 disease modifiers. *Molecular genetics & genomic medicine* 8, e1049–e1049. doi:10.1002/mgg3.1049.
428 31880413[pmid]
- 429 Volden, R. and Vollmers, C. (2021). Highly multiplexed single-cell full-length cdna sequencing of human
430 immune cells with 10x genomics and r2c2. *bioRxiv* doi:10.1101/2020.01.10.902361
- 431 Wang, L., Yu, P., Zhou, B., Song, J., Li, Z., Zhang, M., et al. (2020). Single-cell reconstruction of the adult
432 human heart during heart failure and recovery reveals the cellular landscape underlying cardiac function.
433 *Nature Cell Biology* 22, 108–119. doi:10.1038/s41556-019-0446-7. PMID: 31915373
- 434 Wang, Q., Boenigk, S., Boehm, V., Gehring, N. H., Altmueller, J., and Dieterich, C. (2021). Single cell
435 transcriptome sequencing on the nanopore platform with scsnapbar. *RNA (New York, N.Y.)* 27, 763–770.
436 doi:10.1261/rna.078154.120. PMID: 33906975
- 437 Weeland, C. J., van den Hoogenhof, M. M., Beqqali, A., and Creemers, E. E. (2015). Insights into
438 alternative splicing of sarcomeric genes in the heart. *Journal of Molecular and Cellular Cardiology* 81,
439 107–113. doi:https://doi.org/10.1016/j.yjmcc.2015.02.008. PMID: 25683494
- 440 Wolf, F. A., Angerer, P., and Theis, F. J. (2018). Scanpy: large-scale single-cell gene expression data
441 analysis. *Genome Biology* 19, 15. doi:10.1186/s13059-017-1382-0. PMID: 29409532
- 442 Wu, C.-C., Kruse, F., Vasudevarao, M. D., Junker, J. P., Zebrowski, D. C., Fischer, K., et al. (2016).
443 Spatially resolved genome-wide transcriptional profiling identifies bmp signaling as essential regulator
444 of zebrafish cardiomyocyte regeneration. *Developmental Cell* 36, 36–49. doi:https://doi.org/10.1016/j.
445 devcel.2015.12.010. PMID: 26748692
- 446 Xu, C., Lopez, R., Mehlman, E., Regier, J., Jordan, M. I., and Yosef, N. (2021). Probabilistic harmonization
447 and annotation of single-cell transcriptomics data with deep generative models. *Molecular Systems*
448 *Biology* 17, e9620. doi:https://doi.org/10.15252/msb.20209620. PMID: 33491336
- 449 Zhang, D., Hu, Q., Liu, X., Ji, Y., Chao, H.-P., Liu, Y., et al. (2020). Intron retention is a hallmark and
450 spliceosome represents a therapeutic vulnerability in aggressive prostate cancer. *Nature Communications*
451 11, 2089. doi:10.1038/s41467-020-15815-7. PMID: 32350277
- 452 Zinad, H. S., Natasya, I., and Werner, A. (2017). Natural antisense transcripts at the interface between host
453 genome and mobile genetic elements. *Frontiers in Microbiology* 8. doi:10.3389/fmicb.2017.02292

FIGURE CAPTIONS

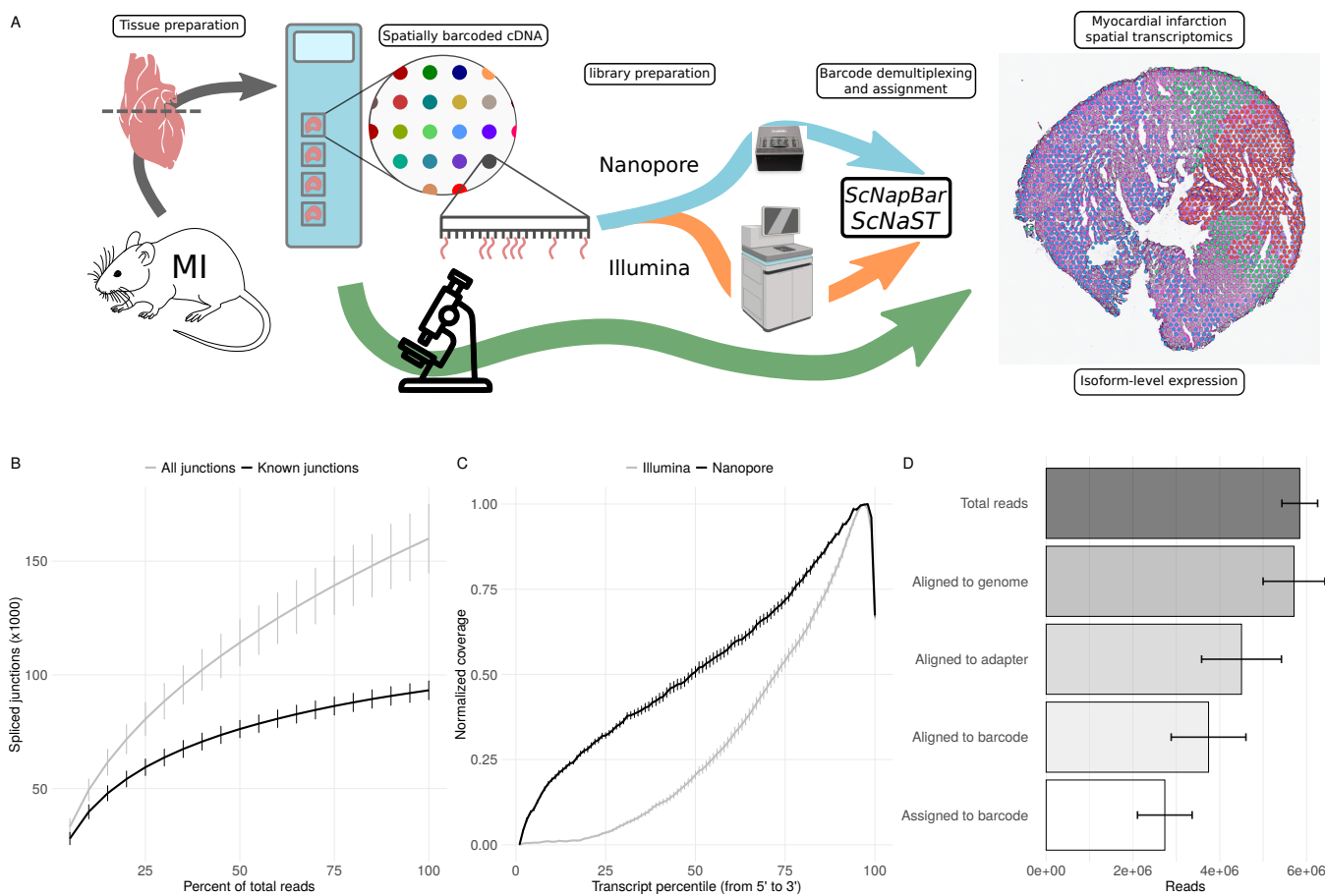


Figure 1. SCNAST methodology. A Schematic of the SCNAST workflow using a hybrid sequencing approach on nanopore and Illumina platforms to assign spatial barcodes to long-read sequencing. B Nanopore sequencing saturation showing the number of splice sites detected at various levels of subsampling. A curve that reaches a plateau before getting to 100% data suggest that all known junctions in the library have been detected. The curve shows the mean \pm SE of four samples. C Normalized transcript coverage for nanopore and Illumina. The curves show the mean \pm SE of four samples. D Reads assigned by SCNAPBAR at each step of the workflow. The bars show the mean \pm SE of four samples.

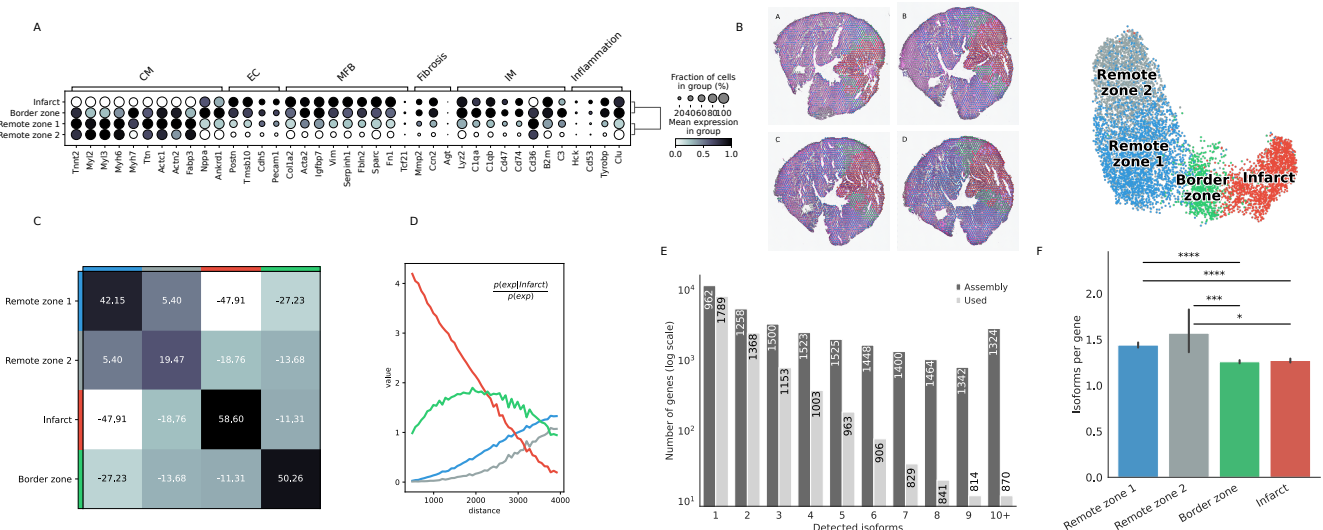


Figure 2. Defining morphological regions after MI. **A** Dot plot showing the expression of selected markers associated with the expression of CM=cardiomyocytes, EC=endothelial cells, MFB=myofibroblasts, IM=immune cells, or with fibrosis and inflammation, based on the short-read Illumina data. **B** Annotation of mouse heart regions after MI via short-read clustering, transferred to the nanopore data. Scatter plot in spatial coordinates of the anatomical regions (left) and UMAP representation of the nanopore data using the region annotation from short-read clustering (right). Colors in the spatial scatter plot are matching those of the UMAP. **C** Neighbors enrichment analysis in one heart axis section. The heatmap shows the enrichment score on spatial proximity between the different anatomical regions. Spots belonging to two different regions that are close together will have a high score, and vice-versa. **D** Cluster co-occurrence in spatial dimensions in one heart axis section. Line plot showing the the conditional probability of observing a given region conditioned on the presence of the infarct region, computed across increasing radii size around each spots. Distance units are given in pixels of the Visium source image. **E** Barplot showing the frequency distribution of the number of isoforms per gene, either stemming from the assembly, or found in the final data after quality control filtering. The median length of transcripts is indicated in each bar for each category. **F** Average number of isoform per gene detected for each morphological region. Significance was measured using a Mann-Witney U-test (** = <0.001, *** = <0.0001)

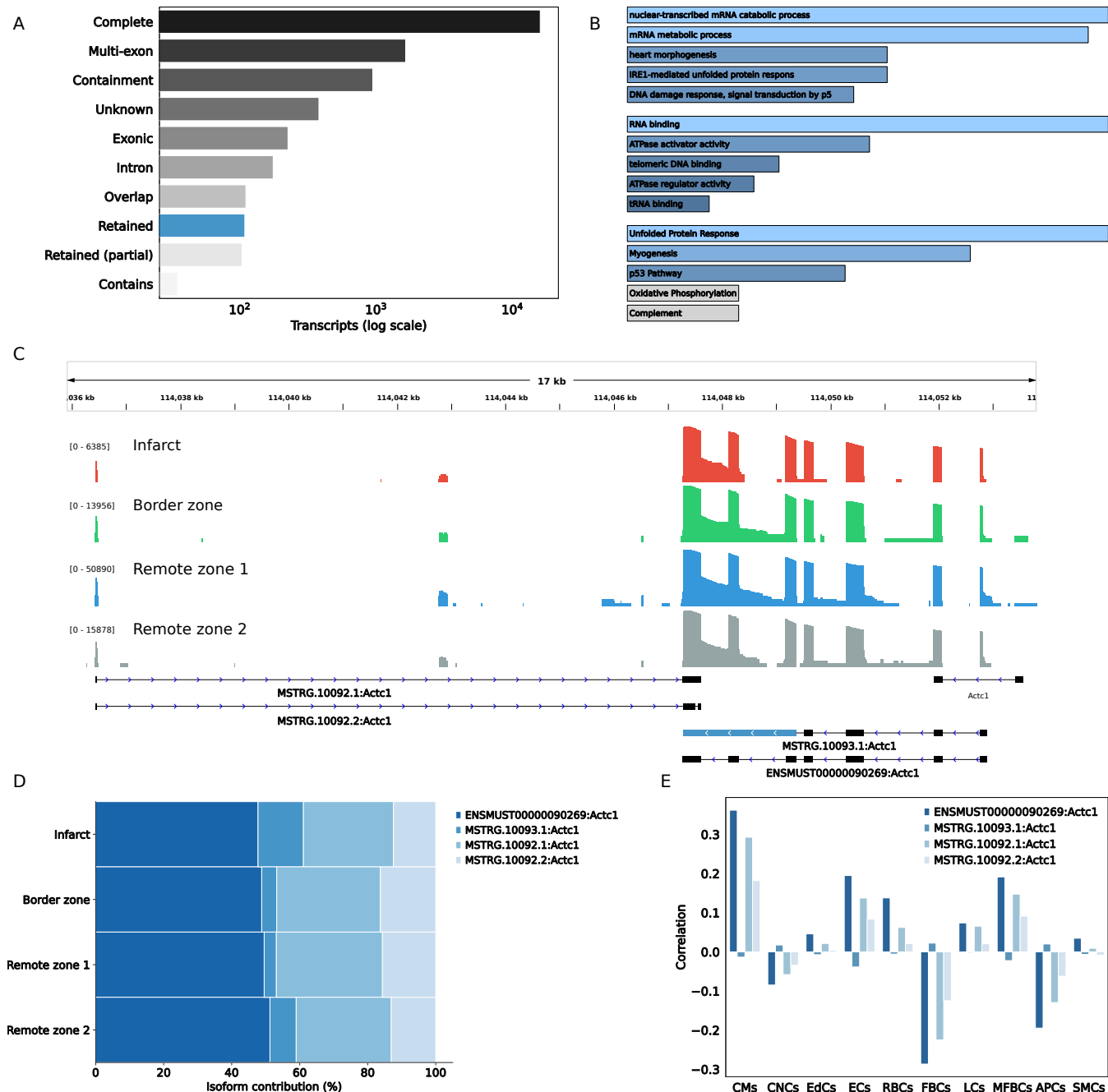


Figure 3. Characterizing the isoform diversity after MI. A Barplot showing how full-length transcripts obtained with scNAST compare to the existing mouse annotation. Labels Complete (=), Multi-exon (j), Containment (k), Unknown (u), Exonic (x), Intron(i), Overlap (o), Retained (m, n), and Contains (y) are explained in <https://ccb.jhu.edu/software/stringtie/gffcompare.shtml>. B Over-representation analysis of genes harboring novel transcripts with intron retention (IR). From top to bottom, biological processes, molecular function, and hallmark gene sets from the Molecular Signatures Database (MSigDB). C Exonic structure of the different *Actc1* isoforms, including novel isoforms identified by scNAST with intron retention and exonic antisense overlap. Coverage (log scale) is shown for each region with a different scale. D *Actc1* isoform contributions to total *Actc1* expression in the different heart regions. E Per spot correlation observed between spatial deconvolution of cell types and *Actc1* isoforms.

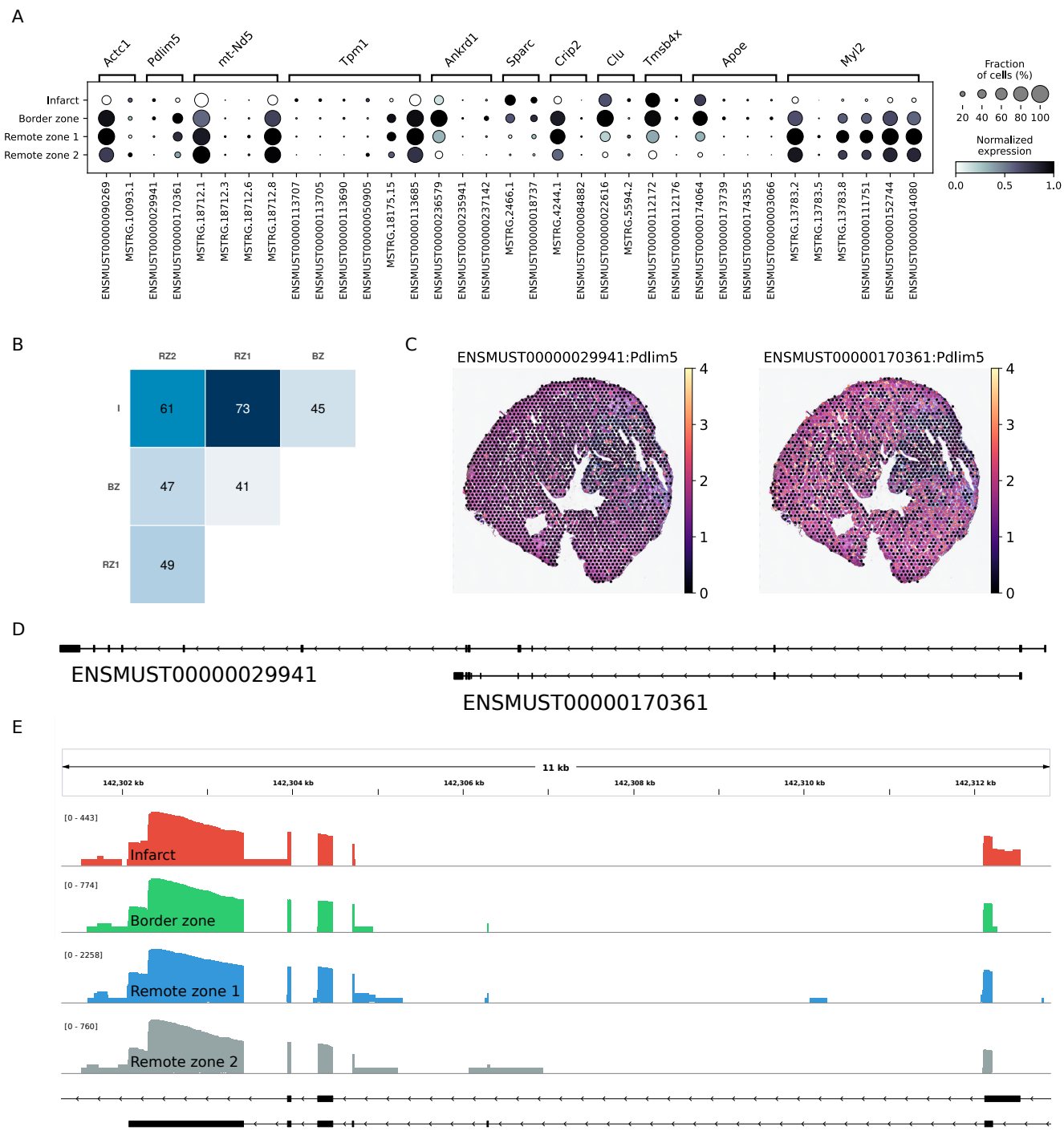


Figure 4. Regional isoform switching after MI. A Dot plot showing the top 5 most significant isoform-switching genes across all comparisons between the remote, border, and infarct areas using a stage-wise testing procedure at an overall false discovery rate (OFDR) of 0.05. The top genes were restricted to those identified as spatially variable. B Heatmap representing the number of isoform-switching genes identified between any two regions. C Pdlim5 isoform expression in one heart axis section. D Pdlim5 isoforms track. E Zoom of D to show coverage of both isoforms across regions.